Evaluation of Electromagnetic Shielding Properties of High-Performance Continuous Carbon Fiber Composites Fabricated by Robotic 3D Printing

Kimia Abedi[1], Seyed Miri[2], Levi Gregorash[2], Kazem Fayazbakhsh[2]*
[1]Department of Mechanical & Industrial Engineering, University of Toronto, Toronto, Ontario, M5S 3G8, Canada
[2]Department of Aerospace Engineering, Ryerson University, Toronto, Ontario, M5B2K3, Canada
*Corresponding author: kazem@ryerson.ca; Tel: (+1) 416-979-5000 ext. 556414; fax: (+1) 416-979-5056; https://orcid.org/0000-0003-3963-8282

Abstract
Fused filament fabrication (FFF) 3D printing can manufacture parts from high-performance continuous carbon fiber composites. In this paper, electromagnetic interference (EMI) shielding effectiveness (SE) of specimens made by robotic 3D printing from low-melt polyaryletherketone (LM PAEK) with continuous carbon fiber (CCF) is investigated. First, a 4-port performance network analyzer with a WR-90 waveguide is used to measure SE in the X-band frequency range (8.2 – 12.4 GHz). Then, unidirectional LM PAEK-CCF specimens with a varying number of layers and fiber orientation are 3D printed. It is found that SE has a linear relation with the number of layers showing maximum total shielding effectiveness (SE_t) of 52.11 dB. Furthermore, as the angle between the electric field and the fibers reduces, there is an increase in the normalized SE_t with respect to thickness with a maximum of 158.4 dB/mm, which is higher than previous values reported in the literature. In addition, pure LM PAEK (AM^{TM} 200) and LM PAEK-CCF specimens are compared, and it is found that CCF reinforcements reduce the resistivity and increase the SE_t of pure LM PAEK by 46 and 38 folds, respectively.

Keywords
Electromagnetic interference shielding; Continuous carbon fiber reinforced composites; Robotic 3D printing; electrical conductivity; shielding effectiveness

Additive Manufacturing Journal
https://doi.org/10.1016/j.addma.2022.102733

1. Introduction

In our modern society, with the increase in the usage and number of electronic devices, the interference of electromagnetic (EM) waves within the same frequency range as the operating frequency is an issue. Notably, in the aerospace industry, high intensity radiated fields surrounding a spacecraft and the onboard electronic equipment concern electromagnetic disturbances that hinder proper operation. The research and development of electromagnetic interference (EMI) shields, then, offers promising prospects [1].

Traditionally, metals' favorable magnetic and electrical properties, including Cu, Ni, Al alloys, etc., allowed them to be used as shields to attenuate the EM waves and protect a device or the internal components against malfunctioning. High electrical conductivity and the existence of a significant number of free electron charge carriers allow metals to rely on reflection as their primary method of shielding [2]. High magnetic permeability, electrical conductivity, and the existence of a significant number of free electron charge carriers allow metals to rely on reflection as their primary method of shielding. Particularly, mobile charge carriers at the surface of a metal contribute to a high impedance mismatch between the sample and air, leading to a significant magnitude of reflection of EM waves [2, 3]. However, high electrical conductivity is not required in a shielding material as electromagnetic waves can also be attenuated through absorption. The attenuation of EM waves by absorption has become an area of focus within industry as reflection-dominated shields usually contribute to secondary EM pollution as the waves are reflected back again into the environment [1]. Thus, researchers have investigated new materials, such as composites with carbon additives, as EMI shields. Implementing carbon fibers (CFs) in a polymeric matrix increases the conductive paths, which leads to increased shielding effectiveness (SE) driven primarily by absorption. Conductive CFs within a polymeric matrix enhances the dielectric permittivity of a specimen allowing the composite to act as an EM absorber as the energy of the EM waves is dissipated through polarization and electrical energy loss. Increasing the CF concentration, optimizing the fiber orientation, and increasing the specimen thickness can increase the EMI shielding absorptive properties of a composite specimen [4]. Carbon-based composite shields offer various advantages, including lower density, higher corrosion resistivity, and higher specific properties than their metallic counterparts [5].

The incorporation of varying types of conductive carbon additives, including continuous carbon fibers (CCFs), carbon nanotubes (CNTs), and graphene derivatives in polymeric matrices, have enhanced the shielding effectiveness of composites [4]. The dispersion of carbon fillers within a matrix, the degree of alignment of fibers, and the concentration of the carbon additives impact the effective conductive networks formed within a matrix, and consequently, the SE [6]. Carbon additives within a polymeric matrix improve the SE by promoting the movement of charge carriers through electron hopping or tunneling once the percolation threshold is reached. The percolation threshold is specified as the critical filler concentration at which the electrical resistivity decreases, and the polymer composite becomes conductive. The filler-to-filler contact at high carbon additive concentrations allows the fillers to coalesce into an interconnective conductive network that assists with charge transport. It is beneficial to achieve high electrical conductivity within a composite at a lower filler concentration as a high percolation threshold restricts the manufacturing flexibility and increases the fabrication costs [4]. Prashantha et al. [7] compared the shielding performance of polylactic acid (PLA) with 10 wt.% graphene to neat PLA. PLA with the graphene additive exhibited an effective SE of 16 dB compared to the 2 dB obtained for the neat one. Chizari et al.

[8] took a similar approach and investigated the impact of CNTs concentration on controllable SE in PLA nanocomposites. The authors emphasized that a positive correlation between the CNT concentration and EMI SE exists, but adding more CNTs beyond the 30 wt.% did not improve the shielding effectiveness. This demonstrates that the relationship between filler concentration and SE will reach a plateau. Moreover, composites with short or continuous carbon fibers have shown effective shielding. Continuous carbon fibers, especially, have higher SE than short fibers due to more uninterrupted conductive networks with a polymer. Increasing the concentration of CCFs compared to randomly oriented or short fibers within a polymeric matrix also enhances the electrical conductivity as the aligned fibers lower the percolation threshold [9]. Thus, polymer composites with CCFs are highly suitable in aerospace due to their effective shielding and high mechanical properties [5].

In addition to the desired properties of carbon allotropes in EMI shielding, carbon-based polymer composites show versatility in their manufacturing methods. Prior experimental work on the shielding effectiveness of carbon fiber composite parts has involved traditional fabrication techniques [10], including foaming, hot pressing, molding, melt compounding, and weaving. Ameli et al. [11] used foam injection molding to fabricate polypropylene carbon fiber (PP-CF) composites. The maximum SE obtained was 7.78 dB/mm attributed to the 10 vol.% CF for a foamed PP-CF specimen tested under the X-band frequency range. Wu et al. [12] used cast molding to fabricate low-density parts with high conductive paths. They incorporated graphene oxide sheets on CFs, and dispersed the fillers in an epoxy resin to achieve an SE of 6.27 dB/mm. Li et al. [13] used the same manufacturing technique to add 15 wt.% long single nano-wall tubes (SNWs) in an epoxy resin, which resulted in an SE of 32.8 dB/mm. Hu et al. [14] also used an epoxy resin with carbonyl iron powders (CIP), and carbon fiber felts to fabricate parts using vacuum molding. Highest SE under the X-band frequency range was attributed to a sample of 0.75 wt.% CIP and 0.75 wt.% carbon fibers with a value of 13.5 dB/mm. To investigate the influence of CCFs on SE, Luo et al. [15] incorporated CCFs at 47 vol.% in epoxy by hot pressing prepreg tapes, allowing a maximum SE of 59.6 dB/mm. Jou et al. [16] developed woven CCF-epoxy composites at 10.8 wt.% CCF through compression molding, which yielded SE values as high as 106 dB/mm.

Additionally, Song et al. [17] took a different approach by maintaining the concentration of CFs and varying the concentration of carbon black (CB) in melt compounded parts to tailor shielding properties. Adjusting the CB concentration from 0 to 15% reduced the electrical resistivity, which in turn increased SE; with five wt.% CF and 15 wt.% CB, an SE of 7.5 dB/mm was obtained. Chung and Eddib [18] used hot pressing of continuous carbon fibers prepreg sheets within polyamide nylon-6 matrix. They tested the conductivity and shielding effectiveness of unidirectional and cross-ply fiber orientation specimens at a frequency of 1 GHz. The results displayed that the conductivity of the longitudinal fibers dominated the conductivity of the whole samples as the longitudinal/transverse conductivity ratio was 930. Thus, shielding by absorption is principally carried out by the fibers parallel to the electric field. Due to the electrical anisotropy of carbon fibers, the layup configuration affected the SE, causing the shielding effectiveness due to absorption, SE_a/thickness, to be higher for a cross-ply composite than its unidirectional counterpart.

As discussed in the current literature, several manufacturing techniques with CCF, including hot pressing or weaving, can fabricate parts with high SE. However, traditional manufacturing techniques do not offer a high degree of freedom in design and cannot manufacture components with complex geometries. Additive manufacturing, called 3D printing, is of increasing interest for manufacturing composite parts. 3D printing processes are ideal due to the ease of fabricating parts with complex geometry and removing the need for a mold or other subtractive machining process [9]. Depending on the application, various process parameters, such as layer height, raster angle, and fiber layup configuration, can be controlled and optimized in 3D printing to achieve a desired EMI shielding effectiveness.

Several researchers have reported enhanced EMI shielding properties of 3D printed polymeric materials reinforced with carbon fibers in the X-band frequency range by altering the process parameters. Yin et al. [20] studied the effect of the number of layers and the raster angle on the SE of 6.41 vol.% CF within a polylactic acid (PLA) matrix. Increasing the number of layers enhanced the SE, while a reduction in SE was seen with an increase in the raster angle. Increasing the number of layers of a PLA composite with carbon material enhances the number of free electron charge carriers and fiber-matrix interactions leading to high shielding performance. They reported a maximized normalized SE value of 15.8 dB/mm for the tested polymeric specimens. Schmitz et al. [21] investigated the impacts of defects and voids on the SE in 3D printed specimens of ABS with five wt.% of CNT. They concluded that lowering the layer height from 0.2 mm to 0.1 mm reduced the SE due to the increased number of formed voids within the 3D printed specimens. The highest reported SE value was 16 dB corresponding to a sample thickness of 2 mm, yielding a normalized value of 8 dB/mm.

Table 1. provides a complete overview of carbon-based composites tested for EMI shielding along with their manufacturing technique. In addition, the results from this study are presented in the last row for a simpler comparison.

Table 1. A review of studies on SE of fiber reinforced composites.

Author	Manufacturing	Polymer	Fibers/fillers	Max. SE (dB)	Thickness (mm)	dB/mm	Range
Prashantha et al. [7]	3D Printing	PLA	10 wt.% CG	16	1.2	13.3	8.2-12.4 GHz (X-Band)
Chizari et al. [8]	3D Printing	PLA	30 wt.% CNT	55	0.4	137.5	8.2-12.4 GHz (X-Band)
Ameli et al. [11]	Foaming	PP	10 vol.% CF	24.9	3.2	7.78	8-12 GHz (X-Band)
Wu et al. [12]	Cast Molding	EP	1.5 mg/mL GO 0.5 wt% CF	37.6	6	6.27	8.2-12.4 GHz (X-Band)
Li et al. [13]	Casting Molding	EP	15 wt.% SWNT	49.2	1.5	32.8	10 MHz-1.5 GHz
Hu et al. [14]	Vacuum Bag Molding	EP	0.75 wt.% CIP 0.75 wt.% CF	53.9	4	13.5	8-12 GHz (X-Band)
Luo et al. [15]	Hot Pressing	EP	47 vol% CCF	124	2.08	59.6	0.3 MHz–1.5 GHz
Jou et al. [16]	Weaving	EP	10.8 wt.% CCF	106	1	106	0.3 – 3 GHz
Song et al. [17]	Melt Compounding	PVDF/PETG	5 wt.% CF 15 wt.% CB	30	4	7.5	0.1 - 1500 MHz
Chung and Eddib. [18]	Hot Pressing	PA6	62 wt.% CCF	66.9	0.966	69.2	0.1 – 1 GHz

Yin et al. [20]	3D Printing	PLA	6.41 vol.% CF	78.9	5	15.8	8-12 GHz (X-Band)
Schmitz et al. [21]	3D Printing	ABS	3.75 wt.% CNT 1.25% CB	16	2	8	8.2-12.4 GHz (X-Band)
Zhao et al. [22]	Weaving	AA	CCF	60.49	1.98	30.6	30 MHz–1.5 GHz
Paddubskaya et al. [23]	3D Printing	PLA	10 wt.% CG	15	1	15.0	26-37 GHz (Ka-Band)
Kotsilkova et al. [24]	3D Printing & Hot Pressing	PLA	10 wt.% CG	15	1	15.0	26-37 GHz (Ka-Band)
Viskadourakis et al. [25]	3D Printing	PLA	Graphene	19	1.2	15.8	3.5-7 GHz (C-Band)
Guan et al. [26]	N/A	N/A	45.1 vol. % NCCF	40.3	1.3	31.0	200-2000 MHz
Lee et al. [27]	3D Printing	PA6	9 vol.% GNP	16	1	16	8.2-12.4 GHz (X-Band)
This study	3D printing	LM PAEK	66 wt.% CCF	60.2	0.38	158.4	8-12 GHz (X-Band)

Polylactic acid (PLA), conductive graphene (CG), carbon nanotube (CNT), polypropylene (PP), carbon fiber (CF), epoxy resin (EP), graphene oxide (GO), single-walled carbon nanotube (SWNT), carbonyl iron powder (CIP), continuous carbon fiber (CCF), poly(vinylidene fluoride) (PVDF), poly(ethylene terephthalateco-1,4-cylclohexylenedimethylene terephthalate) (PETG), polyamide6 (PA6), acrylonitrile butadiene styrene (ABS), carbon black (CB), acrylic adhesive (AA), nickel coated carbon fiber (NCCF), graphene nanoplatelets (GNP), and low-melt polyaryletherketone (LM PAEK).

As shown in Table 1, previous studies on thermoplastic composites investigated the shielding effectiveness of low-temperature polymers with low mechanical performance, like PP, PLA, ABS, and PA6, limiting their application in industry. Here, continuous carbon fiber towpreg with low-melt polyaryletherketone (LM PAEK) is investigated as feedstock for 3D printing, which has superior thermal and mechanical performance over low-temperature thermoplastics. First, specimens from pure LM PAEK and LM PAEK-CCF for electrical conductivity testing are designed and manufactured using a robotic 3D printer. Then, a 0 deg layup with a varying number of layers and a unidirectional design with varying fiber angles are 3D printed for the measurement of EMI shielding effectiveness. Second, the test set-up, including a Vector Network Analyzer (VNA) and a waveguide, is described. The impact of the number of layers and fiber angle on the shielding effectiveness of the 3D printed specimens are evaluated. Finally, the paper wraps up with the main conclusions and directions for future research.

2. Materials and method

In this section, the geometrical dimensions and the layup configuration of the specimens for the electrical conductivity and SE are described. Then, the manufacturing of the samples is discussed, followed by the testing procedure.

2.1. Specimen design and manufacturing

3D printed rectangular samples of 19 mm × 19 mm and 22.86 mm × 10.16 mm (0.9 in. × 0.4 in.) have been investigated for the electrical conductivity and EMI SE characterization, respectively. Two 19 mm × 19 mm samples from pure LM PAEK and LM PAEK-CCF with $[0]_3$ stacking sequence were 3D printed to evaluate the impact of CCF on electrical conductivity. In addition, 13 unique samples of 22.86 mm × 10.16 mm (0.9 in. × 0.4 in.) were manufactured to test the SE based on the number of layers and the raster angles. Six specimens were 3D printed with a various number of layers from one to six. Seven more specimens each with three layers were 3D printed and cut to include raster angles from 0° to 90° in 15° increments, i.e., 0°, 15°, 30°, 45°, 60°, 75°, and 90°. Fiber angle is measured along the length of the specimens and is considered counter-clockwise positive. Table 2 provides an overview of the 3D printed specimens for EMI SE testing.

In the aerospace industry, shield materials have applications in aircrafts and other vehicles with strict weight requirements. Therefore, achieving high shielding capabilities for low-density materials at low thicknesses is desirable. The number of layers has been chosen to vary from one to six to keep the thickness relatively low, below 1 mm, consistent with similar studies on 3D printed specimens [8, 18, 23, 24]. While fiber orientation is limited to 0° or 90° in most studies in the literature [7, 11, 15, 18, 21, 25], it was changed in a 15° increment to explore the impact of the fiber orientation on the SE more precisely. Additionally, one sample has been manufactured for EMI testing for any specific number of layers and fiber orientation. EMI testing is conducted by a network analyzer, which is non-destructive to the samples. In addition, the robotic 3D printing process accurately places fibers in the specimens and prevents inconsistent fiber alignment that might occur in other manufacturing techniques, e.g., compression molding.

Table 2. An overview of the specimens for EMI SE testing.

Specimen set[1]	Test Parameter	Value	Other Parameters
1	Number of Layers (N)	1, 2, 3, 4, 5, 6	θ = 0°
2	Fiber Orientation (θ)	0°, 15°, 30°, 45°, 60°, 75°, 90°	N = 3

[1]Set one incorporates specimens #1 to #6 and set two contains specimens #7 to #13.

A six-axis ABB IRB1200 robotic arm was equipped with a custom-built 3D printing head housing a copper heating block and a slotted nozzle (7 mm × 1.25 mm) to manufacture test specimens on a stainless-steel heated bed. The robotic arm can deposit the materials on the bed per manufacturing and design parameters. A 1/2 in.-thick copper block containing the slotted nozzle was heated to 380 °C using two universal heating elements (24 volts – 50 watts). Its temperature was monitored and controlled through thermocouples and a programmable logic controllers (PLC) box. A stainless-steel plate (101.6 mm × 101.6 mm × 12.7 mm, 4 in. × 4 in. × 1/2 in.) was placed on a larger stainless plate (304.8 mm × 304.8 mm × 12.7 mm, 12 in. × 12 in. × 1/2 in.) which was fitted with a heating pad (110 volts – 500 watts). It was heated to 165 °C while its temperature was monitored and controlled through two thermocouples and a PLC box, respectively. The test specimens have been fabricated from Tenax™-E thermoplastic unidirectional (TPUD) prepreg tape supplied by Teijin Carbon America (Tenax™-E TPUD PAEK-HTS45), which combines carbon fibers with high-performance LM PAEK. The raw prepreg tow contains 12000 carbon filaments and has an overall width of 6.35 mm (1/4 in.) with a nominal thickness of 0.14 mm and a matrix content of 34% by weight. Figure 1 shows the overall 3D printing set-up, including a custom-built 3D printing head, robotic arm, and the heated stainless-steel plate.

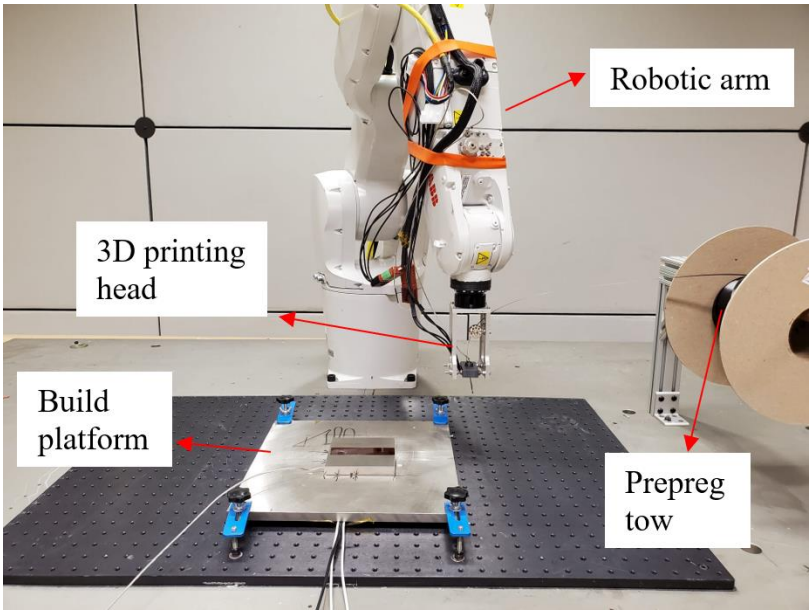

Figure 1. Robotic 3D printer with a custom-built head for processing PAEK-CCF.

G-Codes were created using Cura Lulzbot Edition 4.10 slicer and were converted to the 3D printing paths recognized by the ABB's robotic operating system using RoboDK. The manufacturing and design parameters for 3D printing the specimens were obtained from industry best practices developed in composites automated manufacturing and the physical dimensions of the TPUD prepreg tape (Table 3).

Table 3. Manufacturing and design parameters for 3D printing of specimens.

Printing/Manufacturing Parameter	Value	Printing/Manufacturing Parameter	Value
Build Orientation	XYZ	Nozzle temperature	380 °C
Layer thickness	0.15 mm	Printing speed	5 mm/s
Step width	6 mm	Cooling	No fan cooling
Build platform temperature	165 °C	Infill percentage	100%

Figure 2 shows the 3D printed LM PAEK-CCF specimens with S #1 to #6 corresponding to the first set of specimens with one to six total number of layers, respectively. S #7 to #13 are the second set of specimens with fiber orientation varying from 0° to 90°. S #14 is the specimen with $[0]_3$ stacking sequence used for electrical conductivity measured as mentioned before. After 3D printing, the thickness of specimens was measured in six different points, and the average values were recorded. The average thickness of specimens is: S #1 to #6 (0.14, 0.28, 0.39, 0.61, 0.75, and 0.84 mm), S #7 to #13 (0.35, 0.42, 0.45, 0.44, 0.44, 0.45, and 0.38 mm), and S #14 (0.37 mm).

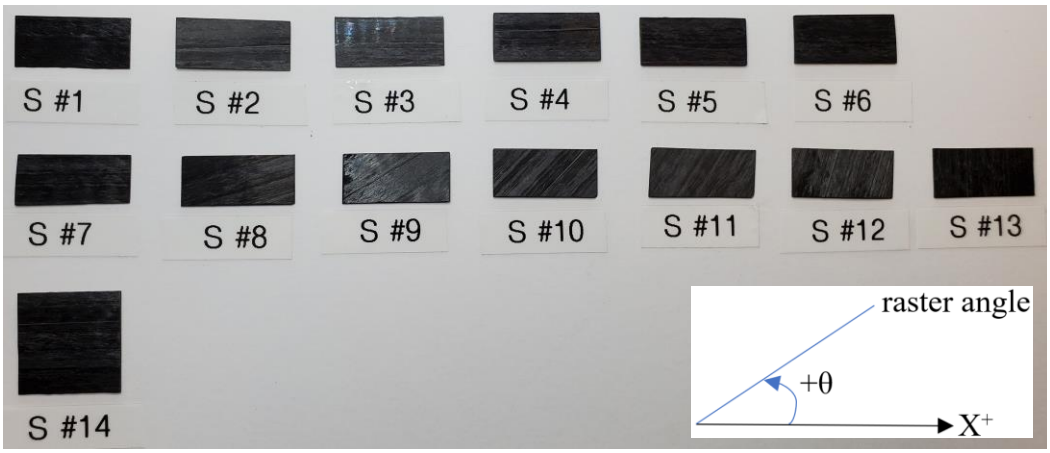

Figure 2. The 3D printed LM PAEK-CCF specimens with a varying number of layers and fiber orientation.

It should be noted that pure LM PAEK specimens were manufactured using a custom-built gantry-based high-temperature 3D printer from AM™ 200 filament, an LMPAEK™ co-polymer, provided by Victrex. It has essentially the same polymer chain as the one in the TPUD prepreg tape for the LM PAEK-CCF specimens. The manufacturing process and design parameters for the pure LM PAEK specimens were the same as the ones summarized in Table 3 for the LM PAEK-CCF samples, except for the following: nozzle temperature, bed temperature, and printing speed of 370 °C, 130 °C, and 40 mm/s, respectively. The AM™ 200 filament and the nozzle diameters were 1.75 mm and 0.6 mm, respectively. Two pure LM PAEK specimens were fabricated: one with a $[0]_3$ stacking sequence for the electrical conductivity measurement with a total thickness of 0.53 mm; and one with a $[0]_6$ stacking sequence for the EMI characterization with a total thickness of 1.04 mm.

2.2. Testing set-up

2.2.1 Electrical conductivity testing

The 3D printed specimens were tested for electrical conductivity using the N1501A dielectric probe kit (Keysight Technologies, Santa Rosa, California, United States) under the X-band frequency range. The high-temperature probe, which features a glass-to-metal seal, was made in contact with the flat surface of each sample to measure the dielectric constant at room temperature. The probe was calibrated in three stages for more accurate measurements using high temperature short, air, and water at 20.3 °C. The dielectric constant of each sample at room temperature was measured using a high-temperature probe, and each measurement was repeated four times to obtain consistent results. The probe measured the real dielectric constant and dielectric loss factor of two 19 × 19 mm LM PAEK and LM PAEK-CCF samples. The conversion of dielectric constant ε' to conductivity σ was performed using angular frequency ω based on the following formula:

$$\sigma = \omega\, \varepsilon' \varepsilon_o \tan\delta \tag{1}$$

where ε_o is the permittivity of free space with an approximate value of $8.85 \times 10^{-12}\ FM^{-1}$, and $\tan\delta$ is the ratio of dielectric loss factor to dielectric constant ($\varepsilon''/\varepsilon'$).

2.2.2 Shielding effectiveness testing

The EMI shielding effectiveness has been measured using a 4-Port Performance Network Analyzer (PNA-X) N5242A (Keysight Technologies, Santa Rosa, California, United States). The overall PNA set-up with the device under test (DUT) is shown in Figure 3. The SE was obtained by measuring the scattering parameters (s-parameters) in the X-Band frequency range (8.2 – 12.4 GHz) using a WR-90 waveguide of dimensions 0.9 in. (Dimension A, 22.9 mm) by 0.4 in. (Dimension B, 10.2 mm) as shown in Figure 4.

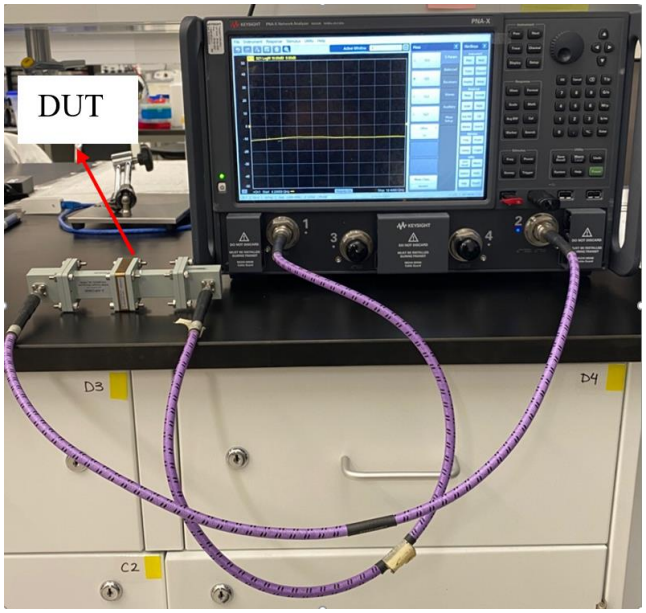

Figure 3. PNA-X N5242A with the two-port set-up and the DUT.

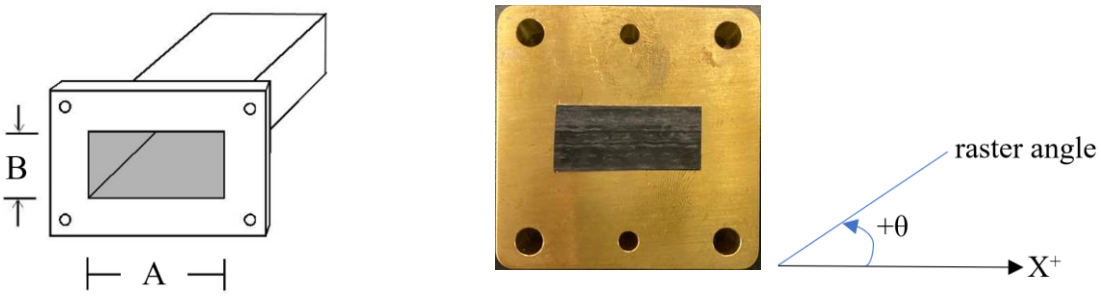

(a) **(b)**

Figure 4. PNA-X N5242A waveguide: (a) CAD drawing with the slot; and (b) the LM PAEK-CCF specimen fitted in the sample holder.

The shielding and attenuation of an incident electromagnetic wave can be carried out by three mechanisms: reflection, absorption, and multiple reflection. All EM waves consist of perpendicular oscillating electric and magnetic fields; therefore, the magnetic and electrical properties of a shielding material play a significant role in wave attenuation primarily by reflection or absorption. In reflection-dominated EMI shielding, with many electron charge carriers within a specimen, an impedance mismatch is generated, reflecting an incident EM wave. Additionally, an induced opposing EM field forms within a specimen as the incident EM field interacts with the

free surface electrons. As a result, the majority of reflection-dominated EMI shields, specifically metals, allow the EM waves to only penetrate through a small depth near the surface, commonly known as the skin depth. At the skin depth, the strength of a field drops to 1/e of its incident surface value. The propagated EM wave may also be partly absorbed, or a small part of it could reflect back and forth between the front and rear end of a specimen, generating multiple internal reflections. In absorption-dominated shielding, the EM waves penetrate through the thickness of the shield due to the lack of a large number of free charge carries on the surface [3]. The shield material then dissipates the absorbed EM waves through dielectric losses, including conductive loss and polarization loss [1].

The total shielding effectiveness, SE_t is the logarithmic ratio of the transmitted power of the EM wave, P_T, to the incident power, P_I, and can also be expressed as the sum of the SE obtained from each shielding mechanism as follows:

$$SE_t = 10 \log\left(\frac{P_T}{P_I}\right) = SE_a + SE_r + SE_m \quad (2)$$

where SE_a, SE_r, and SE_m are shielding effectiveness due to absorption, reflection, and multiple refection, respectively. SE_m is negligible in the calculation of SE_t as it decreases with an increase in the SE_a. According to prior studies, multiple reflection effects in shielding become considerable only when SE_a is below 15 dB [28].

The degree of attenuation of an EM wave by absorption or reflection may be identified from the scattering parameters (S-parameters), which can be used to characterize a two-port network system. A single S-parameter, S_{ij}, characterizes the ratio of the EM wave reflected at port i to the wave incident to port j [29]. SE_a and SE_r can be obtained from S-parameters measured as follows:

$$SE_a = -10 \log\left(\frac{|S_{21}|^2}{1 - |S_{11}|^2}\right) \quad (3)$$

$$SE_r = -10 \log\left(1 - |S_{11}|^2\right) \quad (4)$$

where S_{21} and S_{11} are the transmission and reflection coefficients, respectively [20].

3. Results and discussion

3.1 Electrical Conductivity

Generally, the incorporation of conductive fillers, specifically CCFs, past a critical loading level within an insulating matrix improves the conductivity and dielectric properties. It allows the polymer to transition from insulative to percolative and eventually conductive zones. In composites, electrical conductivity varies based on the type of filler that has been used with the insulating polymeric matrix. Polymeric insulators do not have any free electrons causing their electrical conductivity to be well below 100 S/m. Transition to semi-conductivity occurs at conductivities from 1 S/m to 100 S/m while conductive composites have conductivities ranging from above 100 S/m to 1×10^4 S/m [30]. The electrical conductivity and permittivity are directly correlated to the shielding effectiveness of a composite material. The real electrical permittivity of the LM PAEK and LM PAEK-CCF specimens is illustrated in Figure 5. The real permittivity of the LM PAEK-CCF specimen is much higher than that of LM PAEK, with the former having an average permittivity value of 10.34 compared to 2.06 of the latter. Higher real permittivity causes higher polarization loss resulting in a significant EM absorption within the LM PAEK-CCF specimen. Additionally, the LM PAEK-CCF specimen's conductivity is more enhanced than its

pure LM PAEK counterpart, as a conductivity of 2.37 S/m has been achieved with the former compared to 0.05 S/m for the latter. Thus, the inclusion of CCFs decreases the resistivity by 46 times and transforms the sample from an insulator state to a semi-conductive form. As the electrical resistivity drops, the shielding effectiveness improves due to the interactions between the incident EM wave and the free electrons within the specimen and more conductive networks forming within the polymeric matrix.

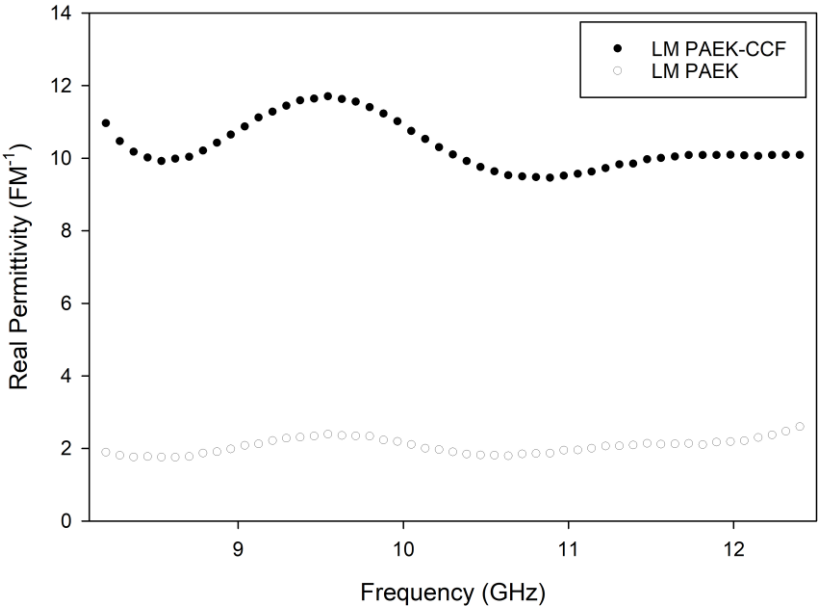

Figure 5. Real electrical permittivity of the LM PAEK-CCF and the LM PAEK specimens within the X-band frequency range.

3.2 EMI shielding effectiveness

3.2.1 Impact of the number of layers on shielding characteristics

The overall shielding effectiveness of the LM PAEK-CCF samples arises from the degree of attenuation of EM waves through absorption and reflection. Figure 6 illustrates the changes in the average SE values with the number of layers. According to the results, there is a direct relation between the number of layers and SE_t. Figure 6 shows an almost linear increase (coefficient of determination, $R^2 = 0.986$) in the average SE_t over the X-band from 11.40 to 52.11 dB as the number of layers within the samples increases from one to six. Therefore, if higher total shielding effectiveness is required for an application, a higher thickness of LM PAEK-CCF will be beneficial. It should be noted that SE_a, SE_r, and SE_t values over the X-band (8.2 – 12.4 GHz) are averaged and plotted in Figure 6, e.g., the average SE_t. The reported trend for the impact of the number of layers on SE_t is consistent with current literature. For example, Yin et al. [20] reported that by adjusting the number of layers in a PLA-CCF specimen, the total SE improved from 25.1 to 69.9 dB.

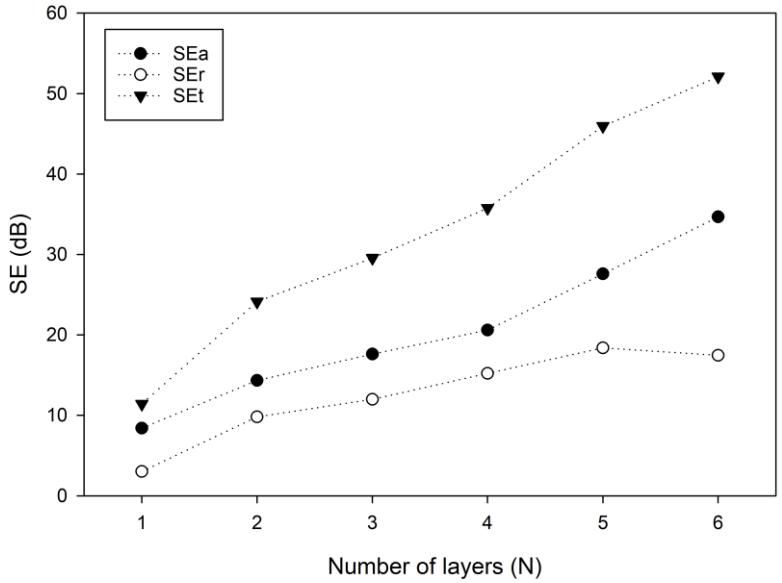

Figure 6. The average SE_a, SE_r, and SE_t with varying number of layers.

It can be observed that shielding dominantly occurs by absorption rather than reflection in all samples. The SE_a significantly increases from 8.39 to 34.67 dB, with an increase in the number of layers from one to six. The degree of attenuation by absorption within a shielding material is subjected to change based on the specimen thickness. Absorption is correlated with ohmic and polarization losses. Therefore, the overall shielding by absorption results from the current flowing through the conductive networks formed by the fibers within the matrix and interfacial polarization, which is related to real permittivity [31]. The contribution of reflection to the total shielding effectiveness ranges between 3.01 and 18.36 dB, depending on the number of layers. With an increase in the total number of layers from one to six, there is 4.13- and 6.10-folds increase in the SE_a and SE_r, respectively. This is in line with results from the literature, where Chung and Eddib [18] reported higher gains in SE_r than SE_a with an increase in the number of layers of a unidirectional composite specimen.

With an increase in the number of layers from one to six, SE_a and SE_t increase; however, SE_r does not raise after five layers. Carbon fibers' quantity, distribution, and orientation remain the same after four layers, resulting in SE_r values with minimal changes. However, the number of mobile charge carriers, and interfaces between carbon fibers and matrix increase with an increase in the number of layers, raising the SE_a [20]. The same trend was observed by Yin et al. [20] where SE_r changes with thickness became minimal after eight layers.

The frequency dependency of SE_a, SE_r, and SE_t in the X-band frequency range is shown in Figure 7.

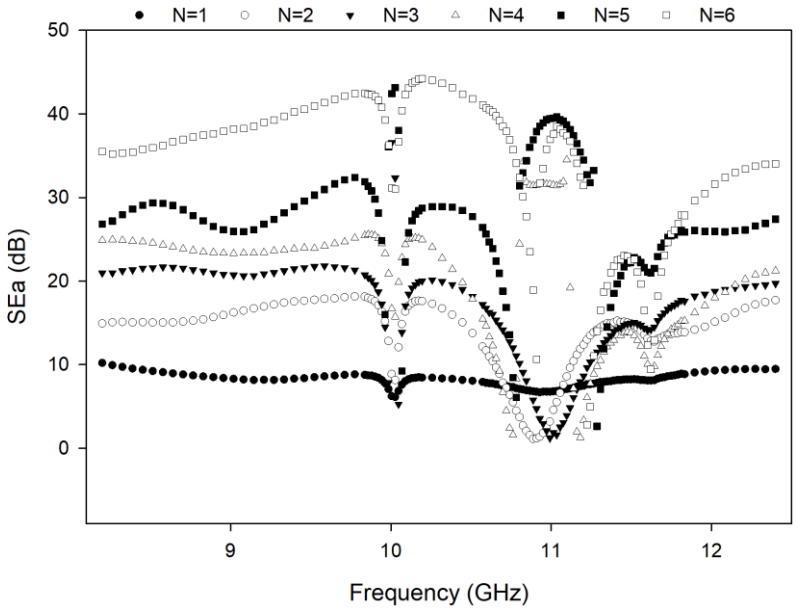
N=1
N=2
N=3
N=4
N=5
N=6
SEa (dB)
Frequency (GHz)

(a)

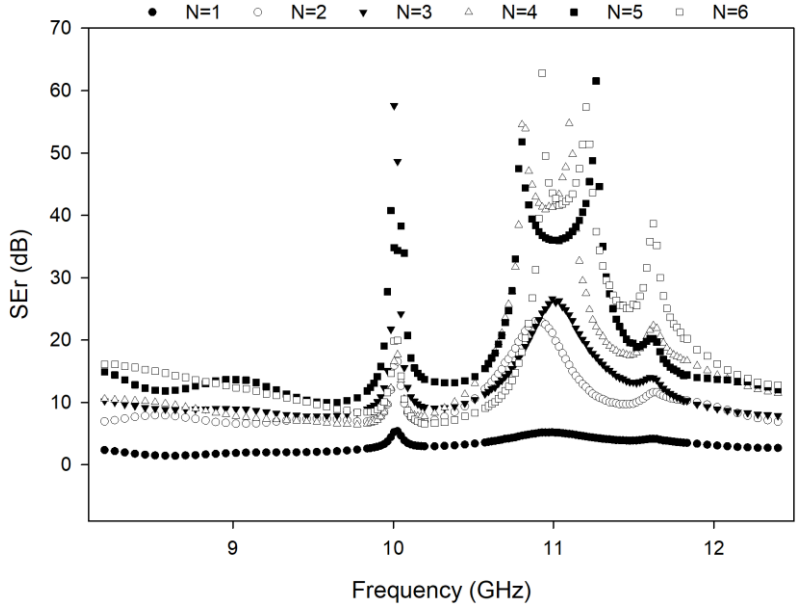
N=1
N=2
N=3
N=4
N=5
N=6
SEr (dB)
Frequency (GHz)

(b)

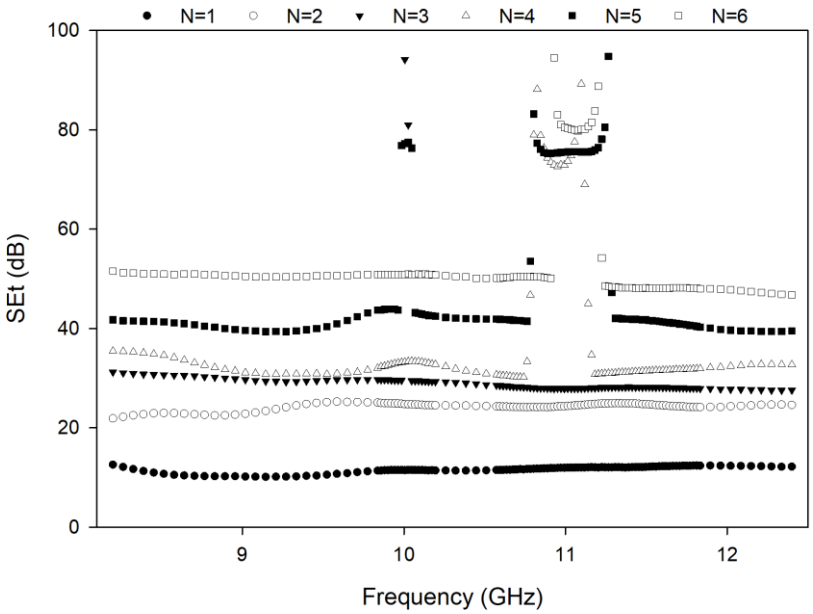

(c)

Figure 7. The variation of shielding with frequency in the LM PAEK-CCF specimens of varying number of layers: (a) SE_a; (b) SE_r; and (c) SE_t.

In general, SE_a, SE_r, and SE_t can be identified through the X-band frequency range, with specimens with a higher number of layers exhibiting higher shielding effectiveness. While changes in the shielding effectiveness for the specimen with one layer are continuous without sudden changes, other specimens showed sharp changes around 10 and 11 GHz. It should be noted that a total of 201 readings were recorded for SE_a, SE_r, and SE_t. In Figure 7, all data points are plotted around 10 and 11 GHz, while only one in every three is shown in other frequencies. LM PAEK-CCF is a dielectric material, and when placed inside an electric field, dielectric polarization occurs. As a result, the specimens resonate with the electromagnetic field and reradiate causing the scatterings. The specimens store energy by shielding due to absorption (Figure 7a), which increases through time and the frequency range. At a certain point, e.g., 10 GHz, the specimen cannot store the extra energy, so it discharges at that frequency, making the specimens transparent, hence the sudden drop in absorption at 10 GHz. Figure 7a shows a material that can have applications as a high Q inductor for specific frequency ranges.

Figure 7c shows that the total shielding effectiveness generally changes less than 10.09 dB in the X-band frequency range, with a sharp increase around 10 and 11 GHz and values as high as 94.80 dB being recorded. Other factors might create scattering in the results, which will require further investigation. For example, shielding effectiveness due to absorption generates heat in the specimens, and the LM PAEK polymer chain might react with the electromagnetic field at specific frequencies. In addition, the 3D printing process induces defects in the form of air porosity in the specimens leading to a random distribution of voids of different sizes in the conducting mesh formed by carbon fibers. The voids can result in an uneven variation of SE_r against frequency [32]. Furthermore, while carbon fibers are oriented at 0° for all specimens, they might not precisely overlap through the specimen thickness, thereby creating lattice-like structures as opposed to a solid surface, which can change the electromagnetic effectiveness at specific frequencies.

3.2.2 Impact of the fiber orientation on shielding characteristics

The second set of specimens (S #7 to #13) have different fiber orientations with the same number of layers, i.e., three; however, there are still some variations in their average thicknesses considering manufacturing tolerances. Therefore, normalized shielding effectiveness with respect to the average specimen thickness (h) is considered in this section. Figure 8 shows changes in the average SE_a/h, SE_r/h, and SE_t/h with fiber orientation increased from 0° to 90°. There is an increase in the shielding effectiveness with an increase in fiber orientation with a maximum value of 158.4 dB/mm at 90°. Carbon fibers in the specimens cut the electric field, and electric charges are displaced along the electric field, causing dielectric polarization, which is the mechanism behind the shielding effectiveness of the specimens. It should be noted that the electric field is along the width of the waveguide (Figure 4a), while the fiber orientation for the specimens is measured along its length (Figure 4b). For the 0° specimen, the electric field is transverse to the carbon fibers; therefore, electric charges can shift slightly along the width of the carbon fibers. As fiber orientation increases, carbon fibers align with the electric field, increasing the range of shift for electric charges, which subsequently increases SE_a/h, SE_r/h, and SE_t/h.

It should be noted that the maximum SE_t/h of 158.4 dB/mm was achieved in this study for S #13, which has an average thickness of 0.38 mm. This shielding effectiveness is higher than previous values reported in the literature (see Table 1), which had a maximum of 137.5 dB/mm for a PLA-CNT specimen with a thickness of 0.4 mm [8]. In addition to the impacts of real permittivity, the formation of interconnective CF network has been partly enabled by utilizing robotic 3D printing to fabricate specimens from CCF prepreg tows. The LM PAEK-CCF specimens have the highest fiber volume fraction of 66% among other studies (see Table 1). The CCFs have a high aspect ratio allowing the charge carries to move through an extended uninterrupted conductive network during polarization. During 3D printing, the unidirectional prepreg tow is passed through the slotted extruder nozzle and is deposited continuously to manufacture the specimens. This results in the length of the CCFs amounting to the length of the specimen, which enhances conductivity. The fabrication of the specimens via 3D printing facilitates higher EM absorption attenuation as the issues with inconsistent filler dispersion and fiber alignment are diminished [9].

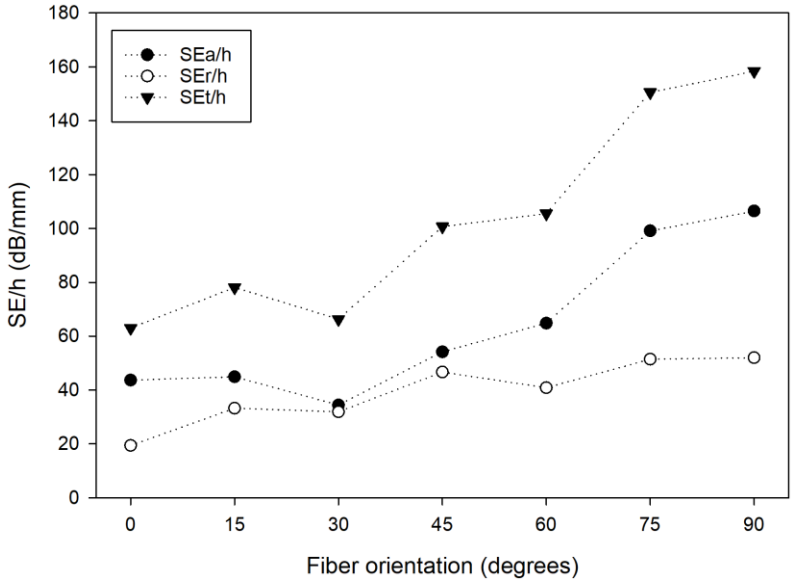

Figure 8. The variation of SE_a/h, SE_r/h, and SE_t/h with varying fiber orientation.

The frequency dependency of SE_a/h, SE_r/h, and SE_t/h for all samples with varying fiber orientation in the X-band frequency range is shown in Figure 9. Like the case of a varying number of layers (Section 3.2.1 and Figure 7), in general, SE_a/h, SE_r/h, and SE_t/h for the specimens with different fiber orientations can be identified through the X-band frequency range, with specimens with higher fiber orientation exhibiting higher shielding effectiveness. Sudden and sharp changes were observed for all the specimens in a frequency range between 10 and 11.5 GHz. Like Figure 7, all data points are plotted around 10 and 11 GHz in Figure 9, while only one in every three is shown in other frequencies. As discussed in Section 3.2.1, resonant cavity and energy discharge can be the reasons behind results scattering. Figure 9c shows that the total normalized shielding effectiveness changes the least for the 0° specimen, while changes are more pronounced for all the other specimens with sharp increases in SE_t between 10 and 11.5 GHz, with values as high as 278.8 dB/mm.

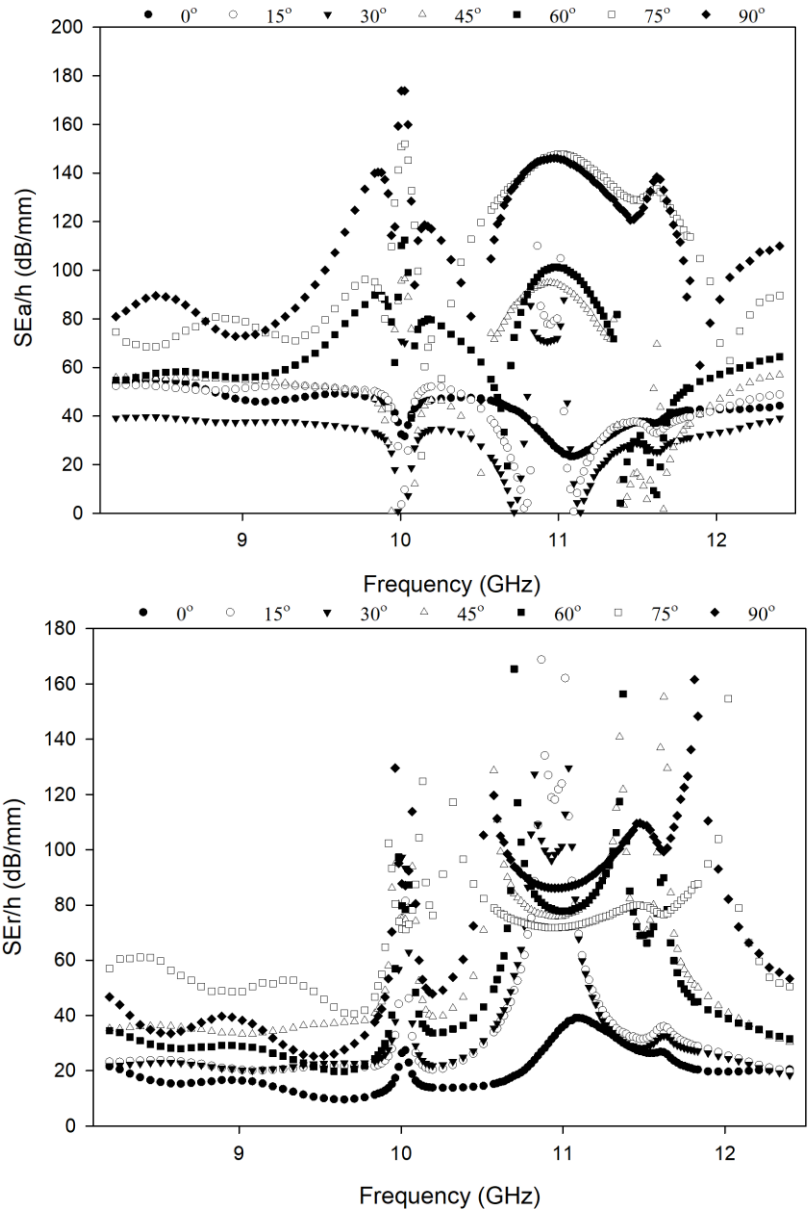

(a)

(b)

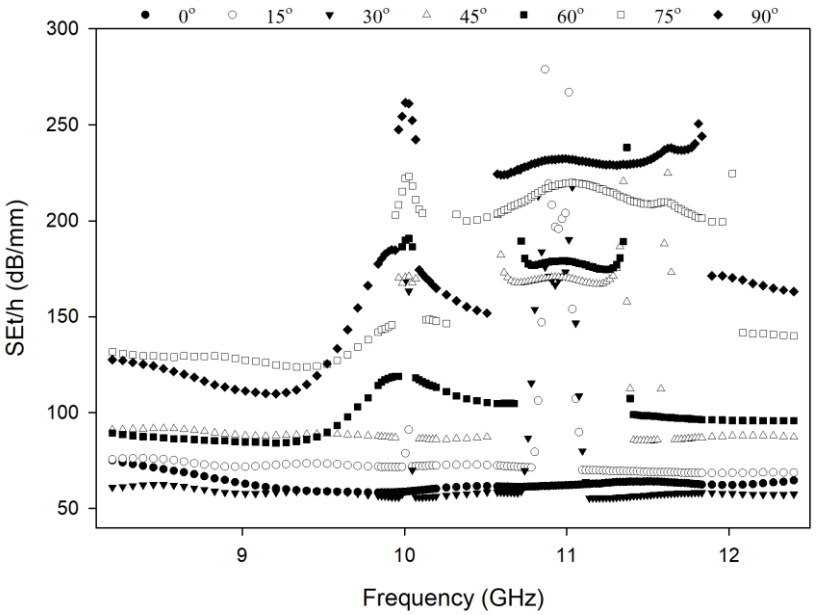

(c)

Figure 9. The variation of shielding with frequency in the LM PAEK-CCF specimens of varying fiber orientation: (a) SE_a/h; (b) SE_r/h; and (c) SE_t/h.

3.3.3 Influence of carbon fiber content on shielding characteristics

Here, the EMI SE of the LM PAEK-CCF samples was measured and compared with their pure LM PAEK counterparts. More specifically, the LM PAEK-CCF sample with $[0]_6$ stacking sequence (S #6) yielded the highest EMI SE in the first set of the specimens; thus, its shielding capabilities were compared to a pure LM PAEK specimen of the same size and number of layers. Figures 10 and 11, respectively, illustrate the average SE values and the SE_t variation with frequency for the specimens. The results show that the LM PAEK-CCF specimen has higher shielding by absorption and reflection compared to the LM PAEK specimen. The LM PAEK-CCF sample exhibited average SE_a, SE_r, and SE_t of 34.66, 17.45, and 52.11 dB, respectively, compared to 0.651, 0.7135, and 1.365 dB obtained for pure LM PAEK. The continuous carbon fibers enhance the overall conductivity and the number of interconnected conductive networks interacting with the incident electromagnetic waves. The LM PAEK-CCF composite specimen performed 38 times better than the pure LM PAEK one in terms of SE_t as conductive carbon fiber networks were formed within the insulating LM PAEK. In addition, the SE_a in the LM PAEK-CCF specimen was higher than the SE_r, indicating the sample was dominantly behaving as an electromagnetic wave absorber. The thickness of the LM PAEK-CCF specimen is lower than the pure PAEK specimen, 0.84 versus 1.04 mm. Therefore, improvements in EMI SE with the introduction of CCFs are even more significant than reported results here if normalized SE values with thickness are considered.

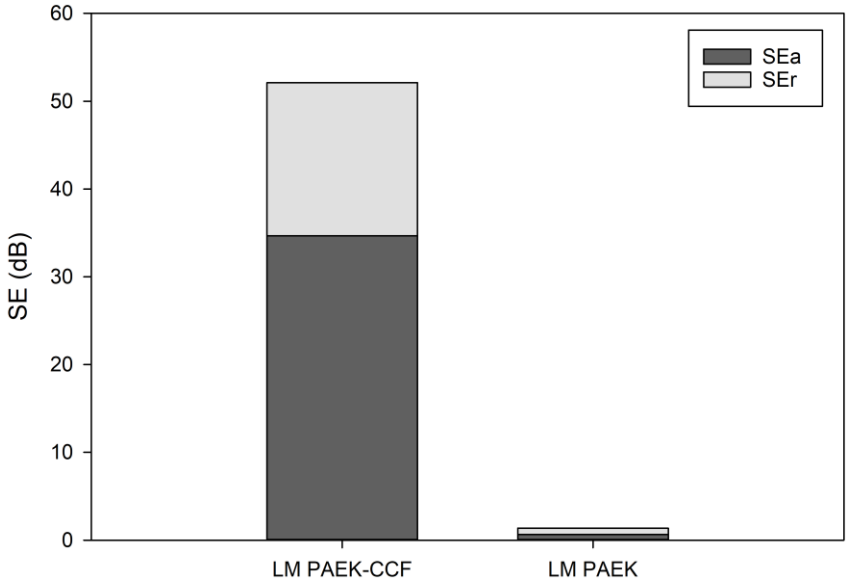

Figure 10. The SE_a, SE_r, and SE_t for the LM PAEK-CCF (S #6) and the LM PAEK specimens.

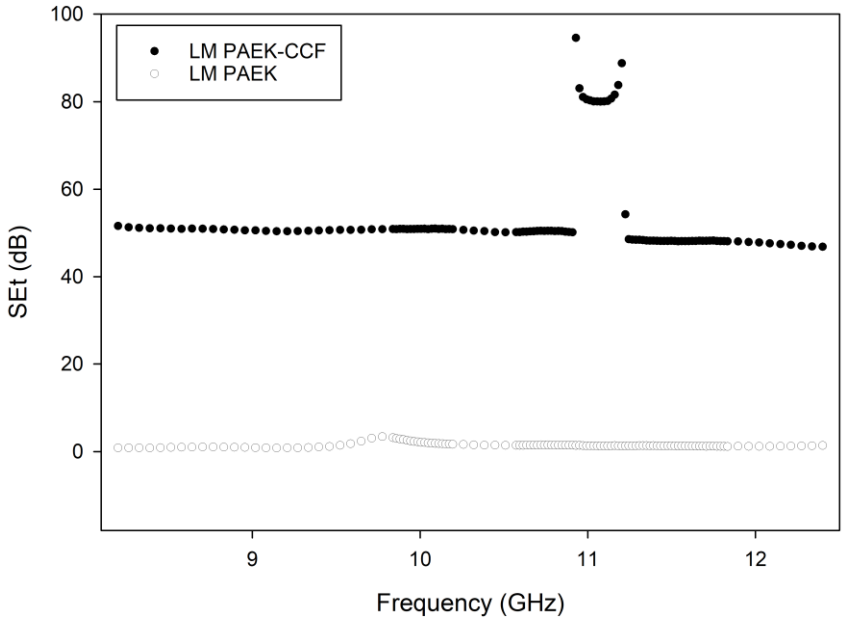

Figure 11. The variation of the SE_t for the LM PAEK-CCF (S #6) and the pure LM PAEK specimens.

4. Conclusions

Electromagnetic shielding effectiveness of high-performance continuous carbon fiber composites was evaluated using a 4-port Performance Network Analyzer in the X-band frequency range (8.2 – 12.4 GHz). Specimens were fabricated using a robotic 3D printer from low-melt polyaryletherketone (LM PAEK) reinforced with continuous carbon fiber (CCF). A total of 13 LM PAEK-CCF specimens were manufactured: six 0° specimens with a varying number of layers from one to six; and seven specimens with three layers and varying fiber orientation from 0° to 90° in 15° increments. With an increase in the number of layers from one to six, results showed an almost linear increase in the average total shielding effectiveness (SE_t) from 11.40 to 52.11 dB. Frequency

dependency of shielding effectiveness by absorption (SE_a), reflection (SE_r), and SE_t showed sharp changes around 10 and 11 GHz. This can be attributed to the dielectric properties of LM PAEK-CCF, generated heat in the specimens during the experiments, and carbon fibers architecture through the thickness of the specimens. For specimens with varying fiber orientation, there was an increase in shielding effectiveness with an increase in the fiber orientation (or a reduction in the angle between the electric field and the fibers) with a maximum of 158.4 dB/mm for the $[90]_3$ specimen. Like specimens with a varying number of layers, sharp changes in shielding effectiveness were observed between 10 and 11.5 GHz. For all the specimens, shielding by absorption was the dominant shielding mechanism. Pure LM PAEK (AM^{TM} 200) and LM PAEK-CCF specimens were compared to investigate the impact of CCF reinforcements on SE. The electrical conductivity of pure LM PAEK and LM PAEK-CCF with a $[0]_3$ stacking sequence were 0.05 and 2.37 S/m, respectively, which showed a reduction in the resistivity by 46 times due to the CCFs. In addition, the pure LM PAEK sample showed SE_a, SE_r, and SE_t of 0.651, 0.7135, and 1.365 dB, respectively, compared to 34.66, 17.45, and 52.11 dB for the LM PAEK-CCF specimen, which showed 38 folds increase in the average total shielding effectiveness due to the inclusion of CCFs.

In this study, SE of unidirectional specimens was investigated, while other layup configurations, e.g., cross-ply, can be explored. In addition, voids in the 3D printed specimens can be measured and their impact on the uneven variation of SE_r against frequency can be explored. Furthermore, complex parts from LM PAEK-CCF can be manufactured using the robotic 3D printer, and its application as a high Q inductor for certain frequency ranges can be investigated.

Acknowledgments
We want to thank Teijin Carbon America and Victrex for providing raw materials, and to acknowledge financial support from the Natural Sciences and Engineering Research Council of Canada (NSERC, RGPIN-2018-04144) and the Ryerson University Faculty of Engineering and Architectural Science Dean's Research Fund. Furthermore, we want to thank Jordan Kalman for 3D printing pure LM PAEK (AM^{TM} 200) specimens, and Dr. Dafna Sussman and Daniel Sare for their help with the calibration and testing of the PNA equipment. Finally, the support from James Millar (CMC Microsystems) and James Dietrich has been instrumental in analyzing the results from this research work and is greatly appreciated.

CRediT author statement
Kimia Abedi: Formal analysis, Investigation, Data Curation, Writing - Original Draft, Writing - Review & Editing. **Seyed Miri:** Investigation, Resources, Writing - Original Draft, Visualization. **Levi Gregorash:** Investigation, Resources, Writing - Original Draft. **Kazem Fayazbakhsh:** Conceptualization, Validation, Resources, Writing - Original Draft, Writing - Review & Editing, Supervision, Project administration, Funding acquisition.

References
[1] Wang M, Tang XH, Cai JH, Wu H, Shen JB, Guo SY. Construction, mechanism and prospective of conductive polymer composites with multiple interfaces for electromagnetic interference shielding: a review. Carbon. 2021 Feb 16.
[2] Chung DD. Materials for electromagnetic interference shielding. Materials Chemistry and Physics. 2020 Jul 25:123587.

[3] Gupta S, Tai NH. Carbon materials and their composites for electromagnetic interference shielding effectiveness in X-band. Carbon. 2019 Nov 1;152:159-87.
[4] Huang Y, Ellingford C, Bowen C, McNally T, Wu D, Wan C. Tailoring the electrical and thermal conductivity of multi-component and multi-phase polymer composites. International Materials Reviews. 2020 Apr 2;65(3):129-63.
[5] Chauhan SS, Abraham M, Choudhary V. Superior EMI shielding performance of thermally stable carbon nanofiber/poly (ether-ketone) composites in 26.5–40 GHz frequency range. Journal of materials science. 2016 Nov;51(21):9705-15.
[6] Chung, D.D.L., 2001. Electromagnetic interference shielding effectiveness of carbon materials. Carbon, 39(2), pp.279-285.
[7] Prashantha, K. and Roger, F., 2017. Multifunctional properties of 3D printed poly (lactic acid)/graphene nanocomposites by fused deposition modeling. Journal of Macromolecular Science, Part A, 54(1), pp.24-29.
[8] Chizari, K., Arjmand, M., Liu, Z., Sundararaj, U. and Therriault, D., 2017. Three-dimensional printing of highly conductive polymer nanocomposites for EMI shielding applications. Materials Today Communications, 11, pp.112-118.
[9] Niendorf K, Raeymaekers B. Additive Manufacturing of Polymer Matrix Composite Materials With Aligned or Organized Filler Material: A Review. Advanced Engineering Materials. 2021 Apr;23(4):2001002.
[10] Advani, S.G. and Hsiao, K.T. eds., 2012. Manufacturing techniques for polymer matrix composites (PMCs). Elsevier.
[11] Ameli, A., Jung, P.U. and Park, C.B., 2013. Electrical properties and electromagnetic interference shielding effectiveness of polypropylene/carbon fiber composite foams. Carbon, 60, pp.379-391.
[12] Wu, J., Chen, J., Zhao, Y., Liu, W. and Zhang, W., 2016. Effect of electrophoretic condition on the electromagnetic interference shielding performance of reduced graphene oxide-carbon fiber/epoxy resin composites. Composites Part B: Engineering, 105, pp.167-175.
[13] Li, N., Huang, Y., Du, F., He, X., Lin, X., Gao, H., Ma, Y., Li, F., Chen, Y. and Eklund, P.C., 2006. Electromagnetic interference (EMI) shielding of single-walled carbon nanotube epoxy composites. Nano letters, 6(6), pp.1141-1145.
[14] Hu, T., Wang, J., Wang, J. and Chen, R., 2015. Electromagnetic interference shielding properties of carbonyl iron powder-carbon fiber felt/epoxy resin composites with different layer angle. Materials Letters, 142, pp.242-245.
[15] Luo, X. and Chung, D.D.L., 1999. Electromagnetic interference shielding using continuous carbon-fiber carbon-matrix and polymer-matrix composites. Composites Part B: Engineering, 30(3), pp.227-231.
[16] Jou, W.S., 2004. A novel structure of woven continuous-carbon fiber composites with high electromagnetic shielding. Journal of electronic materials, 33(3), pp.162-170.
[17] Song, J., Yuan, Q., Zhang, H., Huang, B. and Fu, F., 2015. Elevated conductivity and electromagnetic interference shielding effectiveness of PVDF/PETG/carbon fiber composites through incorporating carbon black. Journal of Polymer Research, 22(8), pp.1-8.
[18] Chung, D.D.L. and Eddib, A.A., 2019. Effect of fiber lay-up configuration on the electromagnetic interference shielding effectiveness of continuous carbon fiber polymer-matrix composite. Carbon, 141, pp.685-691.
[19] Brenken, B., Barocio, E., Favaloro, A., Kunc, V. and Pipes, R.B., 2018. Fused filament fabrication of fiber-reinforced polymers: A review. Additive Manufacturing, 21, pp.1-16.
[20] Yin, L., Tian, X., Shang, Z., Wang, X. and Hou, Z., 2019. Characterizations of continuous carbon fiber-reinforced composites for electromagnetic interference shielding fabricated by 3D printing. Applied Physics A, 125(4), pp.1-11.
[21] Schmitz, D.P., Dul, S., Ramoa, S.D.A.S., Soares, B.G., Barra, G.M.O. and Pegoretti, A., 2021. Effect of printing parameters on the electromagnetic shielding efficiency of ABS/carbonaceous-filler composites manufactured via filament fused fabrication. Journal of Manufacturing Processes, 65, pp.12-19.

[22] Zhao, X., Fu, J. and Wang, H., 2016. The electromagnetic interference shielding performance of continuous carbon fiber composites with different arrangements. Journal of Industrial Textiles, 46(1), pp.45-58.
[23] Paddubskaya, A., Valynets, N., Kuzhir, P., Batrakov, K., Maksimenko, S., Kotsilkova, R., Velichkova, H., Petrova, I., Biró, I., Kertész, K. and Márk, G.I., 2016. Electromagnetic and thermal properties of three-dimensional printed multilayered nano-carbon/poly (lactic) acid structures. Journal of Applied Physics, 119(13), p.135102.
[24] Kotsilkova, R., Ivanov, E., Todorov, P., Petrova, I., Volynets, N., Paddubskaya, A., Kuzhir, P., Uglov, V., Biró, I., Kertész, K. and Márk, G.I., 2017. Mechanical and electromagnetic properties of 3D printed hot pressed nanocarbon/poly (lactic) acid thin films. Journal of Applied Physics, 121(6), p.064105.
[25] Viskadourakis, Z., Vasilopoulos, K.C., Economou, E.N., Soukoulis, C.M. and Kenanakis, G., 2017. Electromagnetic shielding effectiveness of 3D printed polymer composites. Applied Physics A, 123(12), pp.1-7.
[26] Guan, H. and Chung, D.D.L., 2019. Effect of the planar coil and linear arrangements of continuous carbon fiber tow on the electromagnetic interference shielding effectiveness, with comparison of carbon fibers with and without nickel coating. Carbon, 152, pp.898-908.
[27] Lee, K.P.M., Baum, T., Shanks, R. and Daver, F., 2021. Electromagnetic interference shielding of 3D-printed graphene–polyamide-6 composites with 3D-printed morphology. Additive Manufacturing, 43, p.102020.
[28] Zhang, H.B., Yan, Q., Zheng, W.G., He, Z. and Yu, Z.Z., 2011. Tough graphene− polymer microcellular foams for electromagnetic interference shielding. ACS applied materials & interfaces, 3(3), pp.918-924.
[29] Pupalaikis PJ. S-parameters for signal integrity. Cambridge University Press; 2020.
[30] Taherian R, Kausar A. Electrical Conductivity in Polymer-Based Composites: Experiments, Modelling, and Applications. William Andrew; 2018 Nov 30.
[31] Hamidinejad M, Zhao B, Zandieh A, Moghimian N, Filleter T, Park CB. Enhanced electrical and electromagnetic interference shielding properties of polymer–graphene nanoplatelet composites fabricated via supercritical-fluid treatment and physical foaming. ACS applied materials & interfaces. 2018 Aug 20;10(36):30752-61.
[32] Das, N.C., Khastgir, D., Chaki, T.K. and Chakraborty, A., 2000. Electromagnetic interference shielding effectiveness of carbon black and carbon fibre filled EVA and NR based composites. Composites part A: applied science and manufacturing, 31(10), pp.1069-1081.